PHYSICAL REVIEW B VOLUME 9, NUMBER 8 15 APRIL 1974

Two-photon absorption with exciton effect for degenerate valence bands*

C. C. Lee and H. Y. Fan

Department of Physics, Purdue University, West Lafayette, Indiana 47907

(Received 6 August 1973; revised manuscript received 3 December 1973)

Two-photon absorption is treated theoretically using second-order perturbation theory. The exciton effect is taken into account for a crystal with degenerate valence bands. Calculations are made also including another energy band besides the conduction and valence bands. Expressions are given for the absorption of photon pairs from one radiation field and for the absorption of two photons, one from each of two different radiations. Experimental studies are made on ZnTe, GaAs, InP, and InSb. A Nd-glass laser is used for the measurements for ZnTe, GaAs, and InP; measurements on GaAs and InP are also made with the laser in combination with a Hg lamp. InSb is measured with a CO_2 laser. The experimental results are in good agreement with the calculations which take into account the exciton effect for degenerate valence bands, provided the two-photon energy is not too much larger than the energy gap. Calculations show that the degeneracy of valence band is important and that the importance of the exciton effect is larger the bigger the ratio of exciton binding energy to the difference between two-photon energy and the energy gap. These considerations are supported by the experimental results.

I. INTRODUCTION

Multiphoton processes are important at high intensities of radiation and are useful in many applications, for example those involving frequency conversion. Such processes yield information not accessible to one-phonon transitions. Two-photon transitions have been observed in many substances including a number of semiconductors.[1–14] Three types of measurement have been made: transmission, photoconductivity, and luminescence. The two-photon effect was revealed by a dependence on the square of the radiation intensity. Transmision studies on four semiconductors GaAs, InP, InSb, and ZnTe are reported in this paper. A part of the work on GaAs, InP has been reported in a preliminary publication.[11] InP and ZnTe have not been studied by other workers previously. For GaAs and InSb, there is considerable discrepancy among the values of two-photon absorption coefficient over radiation intensity α_2/I reported previously by other groups. The values of α_2/I reported vary from 0.02 to 5.6 cm/MW for GaAs[8–14] and vary from 0.12 to 0.68 cm/MW for InSb.[2–7]

Several theories have been used in calculation of the two-photon effect. Beside a theory[15] based on the consideration of tunneling effect, the others used time-dependent perturbation approach. In using this approach, intermediate states were considered to be associated with a higher lying band in one type of treatment,[16] and intermediate states were taken to be associated with the conduction and valence bands in another type of treatment.[8] The exciton effect was not included in these treatments. It was pointed out in our preliminary report[11] that the calculated value of α_2/I was much lower than the scattered experimental values for GaAs and for InP. The exciton effect was taken into account in treatments[17,18] of two-photon absorption processes for the model of a simple conduction band with a simple valence band. A treatment of a simple conduction band with a degenerate valence band is reported here using the recent theory[19] of exciton states for such a case. Calculations have been made by including another band closest in energy; the results indicate that mainly the conduction band and valence band are important for two-photon absorption in the materials studied. Experimental results obtained with a high-power laser are presented for the four materials. In order to get two-photon energies close to the energy gap E_g of the material, a second light source of variable frequency is used in addition, for GaAs and InP. We conclude that the calculation with exciton effect gives two-photon absorption in good agreement with the experimental results for two-photon energies close to E_g. Discrepancies occur for large differences between the two energies.

II. THEORY

Semiconductors with zinc-blende structure commonly have the maximum of the valence band (VB) at the center of Brillouin zone. The maximum Γ_{15} is triply degenerate, with the heavy hole band V_1, the light hole band V_2, and the spin-orbit-split band V_3.[20] The conduction band (CB) at $\vec{k}=0$ is nondegenerate with Γ_1 representation. Including spin degeneracy, we use $c\alpha$, $c\beta$, to denote the CB and 1α, 1β, ..., 3β to denote the VB. In our treatment, we shall first take into consideration the above-mentioned bands only.

Consider the simultaneous absorption of two photons $\hbar\omega_1$ and $\hbar\omega_2$, where $\hbar\omega_1 < E_g$, $\hbar\omega_2 < E_g$,

$(\hbar\omega_1+\hbar\omega_2)>E_g$. E_g is the energy gap at $\vec{k}=0$, which is assumed to be the energy gap of the semiconductor. The interaction Hamiltonian has the form

$$H=\sum \frac{e}{mc}\,\vec{p}\cdot\vec{A}=\left(\frac{e\mathcal{E}}{2m\omega}\right)^2\sum(\hat{\epsilon}\cdot\vec{p})\,e^{i\vec{K}\cdot\vec{r}} ,$$

where $\vec{p}$ is the electron momentum operator, $\mathcal{E}$ is the electric field of radiation, $\hat{\epsilon}$ is a unit vector parallel to $\mathcal{E}$, and the summation is over all electrons in the valence band of the crystal. In the second-order perturbation theory, the rate of absorption of a photon pair $(\hbar\omega_1+\hbar\omega_2)$ is given by

$$P=\frac{2\pi}{\hbar}\left(\frac{e\mathcal{E}_1}{2m\omega_1}\right)^2\left(\frac{e\mathcal{E}_2}{2m\omega_2}\right)^2\sum_F\left|\sum_I\left(\frac{M_{FI}^{(2)}M_{I0}^{(1)}}{E_I-E_0-\hbar\omega_1}+\frac{M_{FI}^{(1)}M_{I0}^{(2)}}{E_I-E_0-\hbar\omega_2}\right)\right|^2\delta(E_F-E_0-\hbar\omega_1-\hbar\omega_2) , \tag{1}$$

where 1 and 2 refer to the two radiation fields of ω_1 and ω_2, respectively. M_{FI} or M_{I0} is the matrix element of $\sum\hat{\epsilon}\cdot\vec{p}$. The wave vector of radiation $\vec{K}$ is taken to be ~ 0 as is done usually. The indices 0, I, F refer to the initial, the intermediate, and the final states, respectively. The absorption of $\hbar\omega_2$ radiation due to two-photon $(\hbar\omega_1+\hbar\omega_2)$ processes may be characterized by an absorption coefficient

$$\alpha_{1,2}^{(2)}=(8\pi\hbar\omega_2/c\eta_2\mathcal{E}_2^2)P , \tag{2}$$

where η_2 is index of refraction at ω_2. In case of one radiation field $\hbar\omega$, the absorption of radiation due to two-photon $2\hbar\omega$ processes is characterized by the absorption coefficient

$$\alpha_2=(8\pi\hbar\omega/c\eta\mathcal{E}^2)2P . \tag{3}$$

In this case there is only a term under the summation over I in the expression (1) for P.

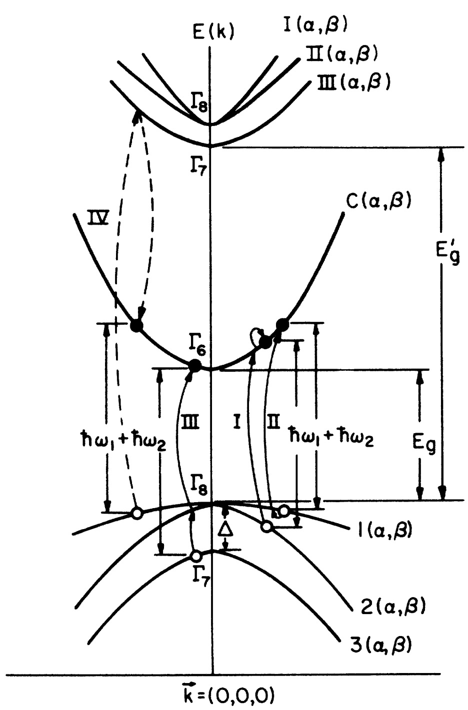

FIG. 1. Schematic diagram of two-photon transition processes. Type-I process involves an intra-conduction-band transition, type-II process involves an intra-valence-band transition, and type III involves an inter-valence-band transition. Type-IV process involves another energy band.

A. Exciton effect neglected

In Fig. 1, three typical two-photon transition processes are shown by arrows. The type-I process involves intra-conduction-band transitions. The type-II process involves intra-valence-band transitions. Type III involves inter-valence-band transitions.

The crystal wave function Ψ is a determinant of single-electron Bloch functions ψ. An interband-transition matrix element between the ground state Ψ_0 and the excited state Ψ' is

$$\langle\Psi'_{i\vec{k},j\vec{k}}|\sum\hat{\epsilon}\cdot\vec{p}|\Psi_0\rangle=\langle\psi_{i\vec{k}}|\hat{\epsilon}\cdot\vec{p}|\psi_{j\vec{k}}\rangle , \tag{4}$$

where $\psi_{j\vec{k}}$ in Ψ_0 is replaced by $\psi_{i\vec{k}}$ in Ψ'. i or j is the band index and $\vec{k}$ is the electron wave vector. An intraband momentum matrix element is

$$\langle\psi_{i\vec{k}}|\hat{\epsilon}\cdot\vec{p}|\psi_{i\vec{k}}\rangle=(m\hbar/m_c)(\hat{\epsilon}\cdot\vec{k}) . \tag{5}$$

The wave functions of the conduction band and the valence band have been given by Kane[21] in the well-known notations

$$\psi_{i\vec{k}}=\varphi_{i\vec{k}}(r)\,e^{i\vec{k}\cdot\vec{r}} , \tag{6}$$

$$\begin{aligned}
\varphi_{c\alpha}&=a_c[iS\downarrow]+b_c[(X-iY)\uparrow/\sqrt{2}]+c_c[Z\downarrow] ,\\
\varphi_{c\beta}&=a_c[iS\uparrow]+b_c[-(X+iY)\downarrow/\sqrt{2}]+c_c[Z\uparrow] ,\\
\varphi_{1\alpha}&=[(X+iY)\uparrow]/\sqrt{2} ,\\
\varphi_{1\beta}&=[(X-iY)\downarrow]/\sqrt{2} ,\\
\varphi_{2\alpha}&=a_2[iS\downarrow]+b_2[(X-iY)\uparrow/\sqrt{2}]+c_2[Z\downarrow] ,\\
\varphi_{2\beta}&=a_2[iS\uparrow]+b_2[-(X+iY)\downarrow/\sqrt{2}]+c_2[Z\uparrow] ,\\
\varphi_{3\alpha}&=a_3[iS\downarrow]+b_3[(X-iY)\uparrow/\sqrt{2}]+c_3[Z\downarrow] ,\\
\varphi_{3\beta}&=a_3[iS\uparrow]+b_3[-(X+iY)\downarrow/\sqrt{2}]+c_3[Z\uparrow] ,
\end{aligned} \tag{7}$$

where the subscripts $c\alpha$, ..., 3β specify the band i. The coefficients a, b, c depend on $\vec{k}$ which is omitted in the subscripts of φ. The basis function X, Y, Z, and S refer to a coordinate system depending on $\vec{k}$. It can be shown that for small values of k, they are approximately

$$a_c=1,\quad b_c=\frac{2^{1/2}}{3}\,\frac{p\hbar k}{mE_g(1+E_g/\Delta)} ,$$

$$c_c = \frac{p\hbar k}{mE_g}\,\frac{E_g + \frac{2}{3}\Delta}{E_g + \Delta}\,, \qquad a_2 = -\left(\tfrac{2}{3}\right)^{1/2} p\hbar k/mE_g\,,$$

$$b_2 = \left(\tfrac{1}{3}\right)^{1/2},\quad c_2 = \left(\tfrac{2}{3}\right)^{1/2},\quad a_3 = \left(\tfrac{1}{3}\right)^{1/2} p\hbar k/m(E_g+\Delta)\,,$$

$$b_3 = \left(\tfrac{2}{3}\right)^{1/2},\quad c_3 = -\left(\tfrac{1}{3}\right)^{1/2}, \tag{8}$$

where

$$p^2 = (\langle iS|\, p_z|\, Z\rangle)^2 = \frac{3m^2}{2}\left(\frac{1}{m_c} - \frac{1}{m}\right)\frac{E_g(E_g+\Delta)}{3E_g + 2\Delta}\,, \tag{9}$$

m_c is the effective mass of the conduction band, and Δ is the spin-orbit splitting of the valence band. Using the wave functions, the momentum matrix elements $\langle\psi_{i\vec{k}}|\,\vec{p}\,|\,\psi_{j\vec{k}}\rangle$ are calculated and listed in Table I. The matrix element between a CB and a VB is approximately independent of k for small values of k; such matrix elements are given for $k=0$.

In the two-photon absorption processes considered, the final state involves a conduction electron and a hole. The electron may be in either one of the conduction bands $c\alpha$ and $c\beta$, and the hole may be in one of the six valence bands. Therefore, there are 12 possible final states. In the intermediate state, the electron may be in one of the two conduction bands and the hole may be in one of the six valence bands. We use i and i' as indices for the conduction bands, j and j' as indices for the valence bands. Replacing the summation over F in Eq. (1) by $\sum_{ij}\int d^3k/(2\pi)^3$, we get

$$P = \sum_{ij}\frac{2\pi}{\hbar}\left(\frac{e\mathcal{E}_1}{2m\omega_1}\right)^2\left(\frac{e\mathcal{E}_2}{2m\omega_2}\right)^2 \times \int \left|\sum_{I}\left(\frac{M_{FI}^{(2)}M_{I0}^{(1)}}{E_I - E_0 - \hbar\omega_1} + \frac{M_{FI}^{(1)}M_{I0}^{(2)}}{E_I - E_0 - \hbar\omega_2}\right)\right|^2 \times \delta(E_F - E_0 - \hbar\omega_1 - \hbar\omega_2)\,\frac{d^3k}{(2\pi)^3}\,. \tag{10}$$

Using the parabolic-band approximation

$$E_c(k) = E_g + \frac{\hbar^2k^2}{2m_c}\,,$$

$$E_j(k) = -\frac{\hbar^2k^2}{2m_{vj}} \qquad \text{for } j = 1\alpha, 1\beta, 2\alpha, 2\beta,$$

$$E_j(k) = -\frac{\hbar^2k^2}{2m_{vj}} - \Delta \quad \text{for } j = 3\alpha,\ 3\beta, \tag{11}$$

we get

$$P = \sum_{ij} P_{ij} = \sum_{ij}\frac{\mathcal{E}_1^2\mathcal{E}_2^2e^4m_{cj}k_j}{64\pi^2m^4\hbar^3\omega_1^2\omega_2^2} \times \int M_{ij}(\vec{k}_j)\sin\theta\, d\theta\, d\phi$$

$$= \sum_{ij}\frac{I_1I_2e^4m_{cj}k_j}{\eta_1\eta_2c^2m^4\hbar^3\omega_1^2\omega_2^2}\int M_{ij}(\vec{k}_j)\sin\theta\, d\theta\, d\phi\,, \tag{12}$$

TABLE I. Momentum matrix element $\langle\psi_{i\vec{k}}|\,\vec{p}\,|\,\psi_{j\vec{k}}\rangle$ for small $\vec{k}$. $\hat{x}'$, $\hat{y}'$, and $\hat{z}'(\parallel\hat{k})$ form a coordinate system according to Kane (Ref. 21).

	$c\alpha$	$c\beta$	1α	1β	2α	2β	3α	3β
$c\alpha$	$\frac{m}{m_c}\hbar\vec{k}$	0	0	$(\frac{1}{2})^{1/2}p(\hat{x}'-i\hat{y}')$	$(\frac{2}{3})^{1/2}p\hat{k}$	$-(\frac{1}{6})^{1/2}p(\hat{x}'+i\hat{y}')$	$-(\frac{1}{3})^{1/2}p\hat{k}$	$-(\frac{1}{3})^{1/2}p(\hat{x}'+i\hat{y}')$
$c\beta$		$\frac{m}{m_c}\hbar\vec{k}$	$(\frac{1}{2})^{1/2}p(\hat{x}'+i\hat{y}')$	0	$(\frac{1}{6})^{1/2}p(\hat{x}'-i\hat{y}')$	$(\frac{2}{3})^{1/2}p\hat{k}$	$(\frac{1}{3})^{1/2}p(\hat{x}'-i\hat{y}')$	$-(\frac{1}{3})^{1/2}p\hat{k}$
1α			$-\frac{m}{m_{v1}}\hbar\vec{k}$	0	0	$-\left(\frac{1}{3}\right)^{1/2}\frac{\hbar kp^2}{mE_g}(\hat{x}'-i\hat{y}')$	0	$\left(\frac{1}{6}\right)^{1/2}\frac{\hbar kp^2m^{-1}}{E_g+\Delta}(\hat{x}'-i\hat{y}')$
1β				$-\frac{m}{m_{v1}}\hbar\vec{k}$	$-\left(\frac{1}{3}\right)^{1/2}\frac{\hbar kp^2}{mE_g}(\hat{x}'+i\hat{y}')$	0	$\left(\frac{1}{6}\right)^{1/2}\frac{\hbar kp^2m^{-1}}{E_g+\Delta}(\hat{x}'+i\hat{y}')$	0
2α					$-\frac{m}{m_{v2}}\hbar\vec{k}$	0	$\left(\frac{2}{9}\right)^{1/2}\left(\frac{1}{E_g}+\frac{1}{E_g+\Delta}\right)\hbar\vec{k}m^{-1}p^2$	$\left(\frac{1}{18}\right)^{1/2}\left(\frac{2}{E_g}+\frac{1}{E_g+\Delta}\right)\hbar km^{-1}p^2(\hat{x}'+i\hat{y}')$
2β						$-\frac{m}{m_{v2}}\hbar\vec{k}$	$-\left(\frac{1}{18}\right)^{1/2}\left(\frac{2}{E_g}+\frac{1}{E_g+\Delta}\right)\hbar km^{-1}p^2(\hat{x}'-i\hat{y}')$	$\left(\frac{2}{9}\right)^{1/2}\left(\frac{1}{E_g}+\frac{1}{E_g+\Delta}\right)\hbar\vec{k}m^{-1}p^2$
3α							$-\frac{m}{m_{v3}}\hbar\vec{k}$	0
3β								$-\frac{m}{m_{v3}}\hbar\vec{k}$

where I_1, I_2 are the radiation intensities and θ, ϕ are the polar angles of $\vec{k}$ vector. The composite two-photon transition matrix element $M_{ij}(\vec{k}_j)$ is defined as

$$M_{ij}(\vec{k}_j) = \left| \sum_{i'j'} \left(\frac{M^{(2)}_{ij,i'j'} M^{(1)}_{i'j',0}}{E_{i'j'} - E_0 - \hbar\omega_1} + \frac{M^{(1)}_{ij,i'j'} M^{(2)}_{i'j',0}}{E_{i'j'} - E_0 - \hbar\omega_2} \right) \right|^2 , \quad (13)$$

$$k_j = [(2m_{cj}/\hbar^2)(\hbar\omega_1 + \hbar\omega_2 - E_g)]^{1/2} \quad \text{for } j = 1\alpha,\ 1\beta,\ 2\alpha,\ 2\beta$$

$$k_j = [(2m_{cj}/\hbar^2)(\hbar\omega_1 + \hbar\omega_2 - E_g - \Delta)]^{1/2} \quad \text{for } j = 3\alpha,\ 3\beta . \quad (14)$$

B. Exciton effect considered

The exciton effect has been considered in two-photon absorption studies for many crystals, without taking into account that the energy bands involved may be degenerate.[17,18] Recently, Baldereschi and Lipari[19] developed a theory of exciton states in semiconductors with degenerate valence bands of the usual type. The theory of two-photon absorption using their treatment of exciton states is developed in the following.

For a conduction band and a degenerate valence band, the wave function of an exciton state may be written as a linear combination of the excited state[22]

$$\Psi_{ijn\vec{K}} = \sum_{\vec{k}} A^{n\vec{K}}_{i\vec{k},(\vec{k}-\vec{K})} \Psi'_{i\vec{k},j(\vec{k}-\vec{K})} , \quad (15)$$

$\vec{K}$ is the exciton wave vector which is equal to the photon wave vector in case of optical excitations and can be neglected. n represents a set of quantum numbers. The coefficients A are given by a Fourier transformation

$$A^{n}_{i\vec{k},j\vec{k}} = V^{-3/2} \int d\vec{r}_e\, d\vec{r}_h\, e^{-i\vec{k}\cdot\vec{r}_e - i\vec{k}\cdot\vec{r}_h} F_{ijn}(\vec{r}_e - \vec{r}_h) , \quad (16)$$

where F_{ijn} is a $\vec{K} = 0$ eigenfunction of the two-particle exciton Hamiltonian in the effective mass formalism. In the Hamiltonian, the Coulomb attraction responsible for the exciton effect is a 6×6 matrix. Baldereschi and Lipari broke down the exciton Hamiltonian into a diagonal and a nondiagonal part. The diagonal part gives eigenstates which have the usual hydrogenic wave functions characterized by a static dielectric constant ϵ_0 and a reduced mass

$$\mu_0 = (1/m_c + \gamma_1/m)^{-1}, \quad (17)$$

γ_1 being one of the usual parameters of the degenerate valence band.[23] The wave functions F_{ij} are the same independent of ij, but the energy is slightly different depending upon whether j refers to v_1, v_2, or the splitoff v_3. The energies calculated for $1s$, $2s$, $2p$ levels are not significantly affected by taking into account the nondiagonal matrix of Coulomb attraction.[24] We shall therefore neglect the effect of the nondiagonal matrix.

Various intermediate states and the final states are exciton states, the final states being the exciton continuum. Referring to Eq. (15), the exciton states involving the same conduction band i and valence band j constitute a series. A discrete state is characterized by a set of quantum numbers whereas a state in the continuum may be characterized by a wave vector

$$\mathcal{K}_j = [(2\mu_0/\hbar^2)(\hbar\omega_1 + \hbar\omega_2 - E_{gj})]^{1/2} . \quad (18)$$

We have in place of Eqs. (12) and (13)

$$P = \sum_{ij} I_1 I_2 \frac{e^4 \mu_0 \mathcal{K}_j}{\eta_1 \eta_2 C^2 m^4 \hbar^3 \omega_1^2 \omega_2^2} \times \int M_{ij}(\vec{\mathcal{K}}_j) \sin\theta\, d\theta\, d\phi , \quad (19)$$

$$M_{ij}(\vec{\mathcal{K}}_j) = \left| \sum_{i'j'n'} \left(\frac{M^{(2)}_{ij\vec{\mathcal{K}},i'j'n'} M^{(1)}_{i'j'n',0}}{E_{i'j'n'} - E_0 - \hbar\omega_1} + \frac{M^{(1)}_{ij\vec{\mathcal{K}},i'j'n'} M^{(2)}_{i'j'n',0}}{E_{i'j'n'} - E_0 - \hbar\omega_2} \right) \right|^2 . \quad (20)$$

The matrix elements in the above equation can be shown to be given by

$$\begin{aligned} M_{i'j'n',0} &= \langle \Psi_{i'j'n'} | \textstyle\sum \hat{\epsilon}\cdot\vec{p} | \Psi_0 \rangle , \\ &= \sqrt{V} F_{i'j'n'}(0) \langle \Psi_{i'0} | \hat{\epsilon}\cdot\vec{p} | \psi_{j'0} \rangle , \end{aligned} \quad (21)$$

$$\begin{aligned} M_{ij\mathcal{K},i'j'n'} &= \left\langle \Psi_{ij\vec{\mathcal{K}}} \right| \textstyle\sum \hat{\epsilon}\cdot\vec{p} \left| \Psi_{i'j'n'} \right\rangle \\ &\simeq \left[\left(\delta_{ii'}\delta_{jj'} \frac{m}{m_c} \right) \hat{\epsilon} - \delta_{ii'} \times \frac{1}{\hbar} \left(\nabla_{\vec{k}} \langle \psi_{j'\vec{k}} | \hat{\epsilon}\cdot\vec{p} | \psi_{j\vec{k}} \rangle_{\vec{k}=0} \right) \right] \\ &\quad \cdot \langle F_{ij\vec{\mathcal{K}}}(\vec{r}) | - i\hbar\nabla_{\vec{r}} | F_{i'j'n'}(\vec{r}) \rangle . \end{aligned} \quad (22)$$

The first term in the square brackets of Eq. (22) involves the effective mass m_c of the conduction band with $\delta_{ii'}$. For $j = j'$, this term and the second term may be considered as representing a transition within one series of the exciton states; they correspond to intra-conduction-band and intra-valence-band transitions, respectively, in the absence of exciton effect. The second term for $j \neq j'$ represents interseries transitions; it corresponds to inter-valence-band transitions. The selection rules for the product of Eq. (21) and the second term of Eq. (22) are determined by the selection rules for the matrix elements of Bloch functions for a degenerate valence band. The allowed combination of (j, j') are indicated by crosses in Table II for $i = c\alpha$. For $i = c\beta$, α and β in Table II should be interchanged. Transitions within one series and transitions involving two different series are shown schematically in Fig. 2 by heavy and thin arrows, respectively.

The energy of exciton states in the continuum can be approximated by

$$E(\mathcal{K}) = E_0 + \hbar^2 \mathcal{K}^2/2\mu_0 \ , \tag{23}$$

irrespective of ij, where E_0 is the lowest energy of the continuum. Using Eqs. (21) and (22) in (20), we get under the summation over $i'j'$ in a matrix element depending on the summation over n':

$$\left\langle F_{\vec{\mathcal{K}}_j}(\vec{r}) \left| \hat{\epsilon}\cdot(-i\hbar\nabla_{\vec{r}}) \right| \sum_{n'} \frac{F_{n'}(r)F^*_{n'}(0)}{E_{n'}-E_0-\hbar\omega} \right\rangle$$

$$\equiv \langle F_{\vec{\mathcal{K}}_j}(\vec{r}) | \hat{\epsilon}\cdot(-i\hbar\nabla_{\vec{r}}) | G(r,0)\rangle \ .$$

In view of Eq. (23), this expression can be shown[18] to be

$$(\hat{\epsilon}\cdot\vec{\mathcal{K}}_j)\frac{\hbar\, e^{X_j\pi/2}\,|\Gamma(2-iX_j)|\, J_j}{(\sqrt{v})E_{bj}} \ , \tag{24}$$

where

$$J_j = 2Y_j^2 \int_0^1 dt\, \frac{t[(1+t)/(1-t)]^{Y_j}}{[1+(tY_j/X_j)^2]^2} \times \exp\left(-2X_j \tan^{-1}\frac{tY_j}{X_j}\right) \ , \tag{25}$$

$$X_j = \left(\frac{E_{bj}}{2\hbar\omega - E_{gj}}\right)^{1/2}, \quad Y_j = \left(\frac{E_{bj}}{E_{gj}-\hbar\omega}\right)^{1/2} , \tag{26}$$

$$E_{bj} = \mu_0 e^4/2\hbar^2\epsilon_0^2 + \Delta E_{dj} \ . \tag{27}$$

E_{bj} is the binding energy of an exciton involving valence band j. The first term of E_{bj} is the binding energy for the case of a simple valence band with an effective mass m/γ_1. The values of E_{dj} have been calculated[19] for many materials including the materials we studied. The integral J_j can be evaluated numerically.[18] Thus we have

$$M_{ij}(\vec{\mathcal{K}}_j) = e^{\pi X_j}|\Gamma(2-iX_j)|^2\left(\frac{J_j}{E_{bj}}\right)^2 \times \left| \langle\psi_{i0}|\hat{\epsilon}\cdot\vec{p}|\psi_{j0}\rangle\left(\frac{\hbar m}{m_{cj}}\hat{\epsilon}\cdot\vec{\mathcal{K}}\right)\right.$$

TABLE II. Selection rules for combinations of j, j' allowed in two-photon transitions, for $i = i' = c\alpha$. The allowed combinations are indicated by crosses.

$j =$	1α	1β	2α	2β	3α	3β
$j' = 1\alpha$						
1β		×	×		×	
2α		×	×		×	×
2β	×			×	×	×
3α		×	×	×	×	
3β	×		×	×		×

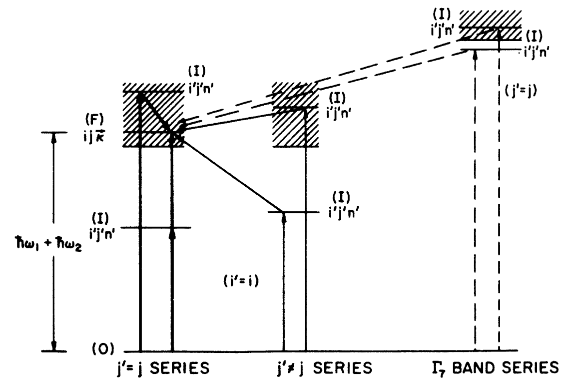

FIG. 2. Two-photon transition processes in the presence of exciton effect. The ground state is denoted by 0, the intermediate states are denoted by I or $i'j'n'$, the final states are denoted by F or $ij\vec{\kappa}$. Transitions within one exciton series and transitions involving two different series are shown by heavy and thin arrows, respectively. Transitions involving the extra band Γ_7 are shown by dashed arrows.

$$\left. - \sum_{j'(\neq j)} \langle\psi_{i0}|\hat{\epsilon}\cdot\vec{p}|\psi_{j'0}\rangle\langle\psi_{j'\vec{\mathcal{K}}}|\hat{\epsilon}\cdot\vec{p}|\psi_{j\vec{\mathcal{K}}}\rangle\right|^2 , \tag{28}$$

where m_{cj} is the combined effective mass of the conduction band and a valence band j. For various ij, $M_{ij}(\vec{\mathcal{K}})$ can be calculated straightforwardly using the momentum matrix elements listed in Table I and taking into account the selection rules listed in Table II. $M_{ij}(\vec{\mathcal{K}})$ can be shown to involve only the angle γ between $\hat{\epsilon}$ and $\vec{\mathcal{K}}$. The transition rate P is obtained by using $M_{ij}(\vec{\mathcal{K}})$ in Eq. (12), bearing in mind that θ and ϕ are the polar angles of $\vec{\mathcal{K}}$.

In the case of a radiation $\hbar\omega_2$ present in addition to the laser radiation $\hbar\omega_1$, we have

$$\langle F_{\vec{\mathcal{K}}}(\vec{r})| -i\hbar\nabla_{\vec{r}}|G_\sigma(r,0)\rangle = \vec{\mathcal{K}}\, \frac{\hbar\, e^{X_j\pi/2}\,|\Gamma(2-iX_j)|\, J_{j,\sigma}}{(\sqrt{v})E_{bj}} \ , \tag{29}$$

$$J_{j,\sigma} = 2Y_{j,\sigma}^2 \int_0^1 dt\, \frac{t[(1+t)/(1-t)]^{Y_{j,\sigma}}}{[1+(tY_{j,\sigma}/X_j)^2]^2} \times \exp\left(-2X_j\tan^{-1}\frac{tY_{j,\sigma}}{X_j}\right) \ , \tag{30}$$

$$X_j = \left(\frac{E_{bj}}{\hbar\omega_1 + \hbar\omega_2 - E_{gj}}\right)^{1/2}, \quad Y_{j,\sigma} = \left(\frac{E_{bj}}{E_{gj}-\hbar\omega_\sigma}\right)^{1/2} \tag{31}$$

in place of Eqs. (24)–(26) for the previous case. $\sigma = 1$, 2 for radiations $\hbar\omega_1$, $\hbar\omega_2$, respectively. We get

$$M_{ij}(\vec{\mathcal{K}}) = e^{\pi X_j}|\Gamma(2-iX_j)|^2 E_{bj}^{-2}$$

$$\times\left|\left[\langle\psi_{i0}|\hat{\epsilon}_i\cdot\vec{p}|\psi_{j0}\rangle\left(\frac{\hbar m}{m_{cj}}\hat{\epsilon}_2\cdot\vec{\mathcal{K}}\right)\right.\right.$$
$$\left.-\sum_{j'(\neq j)}\langle\psi_{i0}|\hat{\epsilon}_1\cdot\vec{p}|\psi_{j'0}\rangle\langle\psi_{j'\vec{\mathcal{K}}}|\hat{\epsilon}_2\cdot\vec{p}|\psi_{j\vec{\mathcal{K}}}\rangle\right]J_{j,1}$$
$$+\left[\langle\psi_{i0}|\hat{\epsilon}_2\cdot\vec{p}|\psi_{j0}\rangle\left(\frac{\hbar m}{m_{cj}}\hat{\epsilon}_1\cdot\vec{\mathcal{K}}\right)\right.$$
$$\left.\left.-\sum_{j'(\neq j)}\langle\psi_{i0}|\hat{\epsilon}_2\cdot\vec{p}|\psi_{j'0}\rangle\langle\psi_{j'\vec{\mathcal{K}}}|\hat{\epsilon}_1\cdot\vec{p}|\psi_{j\vec{\mathcal{K}}}\rangle\right]J_{j,2}\right|^2 . \quad (32)$$

$M_{ij}(\mathcal{K})$ can be shown to involve the angles γ_σ between $\hat{\epsilon}_\sigma$ and $\vec{\mathcal{K}}$, add the angle between $\hat{\epsilon}_1$ and $\hat{\epsilon}_2$. These matrix elements can be combined into three pairs associated respectively with the heavy hole band $v=1$, the light hole band $v=2$, and the split-off band $v=3$. For the case of a laser radiation alone as well as for the case of two radiations, we can write

$$P=\sum_{v=1}^{3} D_v R_v , \quad (33)$$

$$D_v=\left((1+X_v^2)\ \frac{\pi X_v e^{\pi X_v}}{\sinh X_v\pi}\right)\frac{\mu_0^{5/2}}{X_v^3 E_{bv}^{1/2}}\times\frac{\mathcal{E}_1^2\mathcal{E}_2^2 e^4}{2^{3/2}15\pi m^4(\hbar\omega_1)^2(\hbar\omega_2)^2} , \quad (34)$$

$$R_v=[J_{v,1}+J_{v,2}]^2A_v+J_{v,2}B_v , \quad (35)$$

$$A_v=p^2(a_v r_v^2+b_v\rho_2^2+c_v\rho_1^2\rho_2^2+d_v r_v\rho_2+e_v r_v\rho_1\rho_2+f_v\rho_1\rho_2^2) , \quad (36)$$

$$B_v=4p^2\sin^2(\hat{\epsilon}_1,\hat{\epsilon}_2)(a_v^* r_v^2+b_v^*\rho_2^2+c_v^*\rho_1^2\rho_2^2+d_v^* r_v\rho_2+e_v^* r_v\rho_1\rho_2+f_v^*\rho_1\rho_2^2) , \quad (37)$$

where the band parameters involved are

$$p=\langle iS|p_z|Z\rangle, \qquad r_v=m/m_{cv} ,$$
$$\rho_1=E_g/(E_g+\Delta), \quad \rho_2=(p^2/m)/E_g . \quad (38)$$

The numerical coefficients $a, \ldots, f^*$ are listed in Table IV below. In the case of a laser radiation alone,

$$\omega_1=\omega_2=\omega, \quad B_v=0 , \quad (39)$$

P can be shown to be independent of the direction $\hat{\epsilon}$ of radiation polarization. In the case of two beams, P is shown to depend on the angle between $\hat{\epsilon}_1$ and $\hat{\epsilon}_2$ in our model calculation.

If the exciton effect is neglected the following substitution should be made in all the above expressions:

$$(1+X_v^2)\ \frac{\pi X_v e^{\pi X_v}}{\sinh\pi X_v}=1, \quad J_{v,\sigma}=\frac{E_{bv}}{\hbar\omega_1+\hbar\omega_2-\hbar\omega_\sigma} . \quad (40)$$

For $(2\hbar\omega-E_g)$ close to zero the exciton effect increases α_2 by a factor

$$\left((1+X_1^2)\ \frac{\pi X_1 e^{\pi X_1}}{\sinh\pi X_1}\right)\left(\frac{\bar{\imath}\omega J_1}{E_{b1}}\right)^2\left[\sum_v A_v\Big/\sum_v\left(\frac{m_{cv}}{\mu_0}\right)^{5/2}A_v\right], \quad (41)$$

where $(\hbar\omega J_1/E_{b1})$ is close to unity. The factor in the first large parentheses close to unity for $X_1\equiv[E_{b1}/(2\hbar\omega-E_g)]^{1/2}<\pi^{-1}$ and increases rapidly for larger X_1, showing that large E_b and small $(2\hbar\omega-E_g)$ make the exciton effect important. For the case of a simple valence band, the factor in large square brackets reduces to unity. This factor is the larger the smaller the weighted average of $m_{cv}/\mu_0\equiv(1+\gamma_1 m_c/m)/(1+m_c m_v)$. For one-photon absorption, the exciton effect increases the absorption coefficient simply by a factor[25] $(\pi X e^{\pi X}/\sinh\pi X)$. The exciton effect is more important for α_2 since it affects also the intermediate states.

In the case of a nondegenerate valence band, there is one parameter m_{cv} and one factor A. Compare to A_v's, A is simplified by the omission of inter-valence-band terms. In the presence of exciton effect, degeneracy of valence band increases α_2 by the factor

$$\left[\sum_v \mu_0^{5/2}A_v\Big/m_{cv}^{5/2}A\right] . \quad (42)$$

For a nondegenerate band which resembles v_1 of the degenerate bands, A is smaller than A_v, $\mu_0\sim m_{cv}$, and the value of this factor is >2.

C. Effect of other energy bands

The effect of another energy band is the larger the closer the band in energy to the conduction band or valence band. In order to assess the effect of other energy bands, we consider a band closest in energy. In the materials studied, such a band is Γ_{15} above the conduction band. The Γ_{15} band is triply degenerate. Including spin, Γ_{15} becomes a fourfold degenerate Γ_8 and a double degenerate Γ_7. The Γ_7 lies lower in energy by spin-orbit splitting. The four wave functions of Γ_8 are

$$\varphi_{\mathrm{I}\alpha}=[(x+iy)\uparrow/\sqrt{2}] ,$$
$$\varphi_{\mathrm{I}\beta}=[(x-iy)\downarrow/\sqrt{2}] ,$$
$$\varphi_{\mathrm{II}\alpha}=[(1/\sqrt{6})(x-iy)\uparrow+\sqrt{\tfrac{2}{3}}\,z\downarrow] ,$$
$$\varphi_{\mathrm{II}\beta}=[-(1/\sqrt{6})(x+iy)\downarrow+\sqrt{\tfrac{2}{3}}z\uparrow],$$

and the two wave functions of Γ_7 are

$$\varphi_{\mathrm{III}\alpha}=[(1/\sqrt{3})(x-iy)\uparrow-(1/\sqrt{3})z\downarrow] ,$$
$$\varphi_{\mathrm{III}\beta}=[-(1/\sqrt{3})(x+iy)\downarrow-(1/\sqrt{3})z\uparrow] , \quad (43)$$

where x, y, z are the basis functions of Γ_{15} in the same coordinate system as that used in Eq. (7). The calculated momentum matrix elements[26] connecting Γ_{15} with the conduction and valence bands are listed in Table III where

TABLE III. Momentum matrix element between CB, VB, and the next higher band Γ_{15} at Γ point.

	$\mathrm{I}\alpha$	$\mathrm{I}\beta$	$\mathrm{II}\alpha$	$\mathrm{II}\beta$	$\mathrm{III}\alpha$	$\mathrm{III}\beta$
$c\alpha$	0	$(\frac{1}{2})^{1/2}p'(\hat{x}'-i\hat{y}')$	$(\frac{2}{3})^{1/2}p'\hat{z}'$	$-(\frac{1}{6})^{1/2}p'(\hat{x}'+i\hat{y}')$	$-(\frac{1}{3})^{1/2}p'\hat{z}'$	$-(\frac{1}{3})^{1/2}p'(\hat{x}'+i\hat{y}')$
$c\beta$	$(\frac{1}{2})^{1/2}p'(\hat{x}'+i\hat{y}')$	0	$(\frac{1}{6})^{1/2}p'(\hat{x}'-i\hat{y}')$	$(\frac{2}{3})^{1/2}p'\hat{z}'$	$(\frac{1}{3})^{1/2}p'(\hat{x}'-i\hat{y}')$	$-(\frac{1}{3})^{1/2}p'\hat{z}'$
1α	0	0	$-(\frac{1}{3})^{1/2}Q\hat{z}'$	$-(\frac{1}{3})^{1/2}Q(\hat{x}'+i\hat{y}')$	$-(\frac{2}{3})^{1/2}Q\hat{z}'$	$(\frac{1}{6})^{1/2}Q(\hat{x}'+i\hat{y}')$
1β	0	0	$(\frac{1}{3})^{1/2}Q(\hat{x}'-i\hat{y}')$	$-(\frac{1}{3})^{1/2}Q\hat{z}'$	$-(\frac{1}{6})^{1/2}Q(\hat{x}'-i\hat{y}')$	$-(\frac{2}{3})^{1/2}Q\hat{z}'$
2α	$(\frac{1}{3})^{1/2}Q\hat{z}'$	$-(\frac{1}{3})^{1/2}Q(\hat{x}'+i\hat{y}')$	0	0	0	$-(\frac{1}{2})^{1/2}Q(\hat{x}'-i\hat{y}')$
2β	$(\frac{1}{3})^{1/2}Q(\hat{x}'-i\hat{y}')$	$(\frac{1}{3})^{1/2}Q\hat{z}'$	0	0	$-(\frac{1}{2})^{1/2}Q(\hat{x}'+i\hat{y}')$	0
3α	$(\frac{2}{3})^{1/2}Q\hat{z}'$	$(\frac{1}{6})^{1/2}Q(\hat{x}'+i\hat{y}')$	0	$(\frac{1}{2})^{1/2}Q(\hat{x}'-i\hat{y}')$	0	0
3β	$-(\frac{1}{6})^{1/2}Q(\hat{x}'-i\hat{y}')$	$(\frac{2}{3})^{1/2}Q\hat{z}'$	$(\frac{1}{2})^{1/2}Q(\hat{x}'+i\hat{y}')$	0	0	0

$$p'=\langle z|\,p_z\,|iS\rangle,\quad Q=i\langle X|\,p_z\,|y\rangle\ . \tag{44}$$

The composite transition matrix element given by Eq. (13) involves now additional intermediate states contributed by the extra band. It may be written symbolically as

$$M_{ij}(k)=\left|\sum_{i'j'}(C,V)+\sum_{i'j'}(C,V,\Gamma_{15})\right|^2 . \tag{45}$$

The first term of the quantity to be squared is due to intermediate states associated with CB and VB, and the second term is due to intermediate states associated with Γ_{15} and VB. A transition process contained in the second term involving the extra band is shown in Fig. 1 by dashed arrows. We shall consider the case of laser radiation alone. Equation (33) for the rate of transition is replaced by

$$P=\sum_{v=1}^{3}(D_vR_v+D'_vR'_v)\ . \tag{46}$$

$D'_vR'_v$ represents the effect of the presence of the Γ_{15} band.

If the exciton effect is neglected, we get

$$D'_v=\frac{(2\hbar\omega-E_{gv})^{1/2}}{E'_{gv}-\hbar\omega}\ \frac{m_{cv}^{5/2}\mathcal{E}^4e^4}{2^{5/2}15\pi m^4(\hbar\omega)^4}\ , \tag{47}$$

$$R'_v=\frac{p'Q}{m_{cv}}\left(a'_v\frac{p'Q}{E'_{gv}-\hbar\omega}+(b'_v r_v+c'_v\rho_2+d'_v\rho_1\rho_2)\times\frac{p(2m_{cv})^{1/2}(2\hbar\omega-E_{gv})^{1/2}}{\hbar\omega}\right)\ . \tag{48}$$

The values of a'_v, ..., d'_v are listed in Table IV with

TABLE IV. Coefficients defined in Eqs. (36), (37), (48), and (51). $N=\cos(\hat{\epsilon}_1,\hat{\epsilon}_2)$, $n=\cos(\hat{\epsilon},\hat{z})$.

v	a	b	c	d	e	f
1	$(2-N^2)$	$\frac{1}{9}(11-3N^2)$	$\frac{5}{9}$	$\frac{2}{3}(3N^2-1)$	$\frac{1}{3}(3N^2-1)$	$\frac{2}{9}(1-3N^2)$
2	$\frac{1}{3}(4+3N^2)$	$\frac{1}{54}(49+203N^2)$	$\frac{5}{54}(5+N^2)$	$\frac{16}{9}(3N^2-1)$	$\frac{7}{9}(3N^2-1)$	$\frac{1}{27}(27+49N^2)$
3	$\frac{5}{3}$	$\frac{1}{27}(N^2+5)$	$\frac{10}{27}(1+5N^2)$	$\frac{10}{9}(3N^2-1)$	$\frac{10}{9}(3N^2-1)$	$\frac{10}{27}(3+5N^2)$
	a^*	b^*	c^*	d^*	e^*	f^*
1	$-\frac{5}{4}$	$-\frac{5}{9}$	$-\frac{5}{36}$	$\frac{5}{3}$	$\frac{5}{6}$	$-\frac{5}{9}$
2	$-\frac{5}{12}$	$-\frac{20}{27}$	$-\frac{5}{12}$	$\frac{10}{9}$	$\frac{5}{6}$	$-\frac{10}{9}$
3	$-\frac{5}{6}$	$-\frac{5}{6}$	$-\frac{10}{27}$	$\frac{5}{3}$	$\frac{10}{9}$	$-\frac{10}{9}$
	a''	b''	c''	d''	e''	f''
1	$\frac{5}{3}$	$\frac{1}{2}(5n^4-1)$	$\frac{1}{18}(25n^4+30n^2-13)$	$\frac{1}{9}(10n^4-15n^2+2)$		
2	$\frac{5}{3}$	$\frac{1}{6}(5n^4-1)$	$\frac{1}{18}(-15n^4+150n^2-47)$	$\frac{1}{9}(5n^4+15n^2-6)$		
3	0					
	a'	b'	c'	d'		
1	4	$5(n^4-1)$	$\frac{2}{3}(5n^4-1)$	$\frac{1}{3}(5n^4-1)$		
2	$\frac{1}{3}(9+30n^2-35n^4)$	$-\frac{4}{3}$	0	$\frac{4}{9}$		
3	$\frac{1}{6}(21+30n^2-35n^4)$	$\frac{2}{3}(1-5n^4)$	$\frac{2}{9}(1-5n^4)$	0		

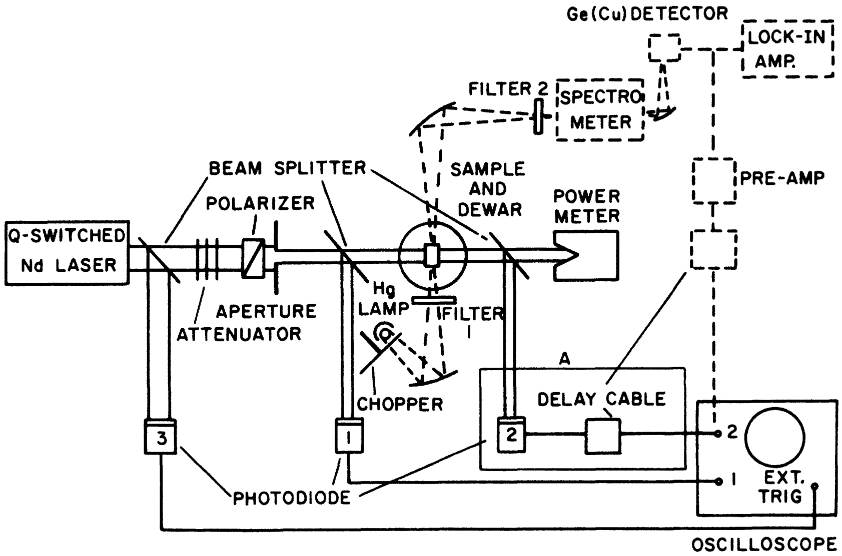

FIG. 3. Experimental arrangement with the Nd-glass laser alone is shown by solid lines. In the measurements using an additional light source, the part enclosed in A is replaced by the part shown by dashed lines.

prime referring to Γ_{15} band.

In taking into account the exciton effect, we shall for simplicity consider only Γ_7 as the extra band, in which case the treatment of exciton states is similar to that for the combination of conduction band and degenerate valence band. Transitions involving the extra band are shown schematically in Fig. 2 by the dashed arrows. The expressions for $M_{i'j'n',0}$ given by (21) is applicable to the extra intermediate exciton states also. Instead of (22), the matrix element connecting an extra intermediate state with a final state is given by

$$M_{ij\vec{K},i'j'n'} = \delta_{jj'}\langle\psi_{i0}|\hat{\epsilon}\cdot\vec{p}|\psi_{i'0}\rangle\langle F_{ij\vec{K}}|F_{i'j'n'}\rangle \ . \tag{49}$$

The second term in the square brackets of Eq. (22) vanishes on account of $\langle\varphi_{i\vec{k}}|\varphi_{i'\vec{k}}\rangle = 0$ for two different bands. Using Eqs. (21) and (49), we get

$$D_v' = \tfrac{1}{2} D_v\left(\frac{X_v^2}{1+X_v^2}\,\frac{E_{bv}}{E_{gv}'-\hbar\omega}\right) \ , \tag{50}$$

$$R_v' = \frac{p'Q}{\mu_0}\left[a_v''\,\frac{p'Q}{E_{gv}'-\hbar\omega} + (b_v''r_v + c_v''\rho_2 + d_v''\rho_1\rho_2) \times\left(\frac{2\mu_0 J_v^2}{E_{bv}}\,\frac{1+X_v^2}{X_v^2}\right)^{1/2} p\right] \ . \tag{51}$$

The values of a_v'', ..., d_v'' can be found in Table IV with double prime referring to Γ_7 band. If the exciton effect is neglected, the following substitutions should be made in (50) and (51):

$$\frac{\pi X_v e^{\pi X_v}}{\sinh \pi X_v} = 1, \quad J_v = \frac{E_{bv}}{\hbar\omega}, \quad \mu_0 = m_{cv} \ , \tag{52}$$

giving results which agree with (47), (48) reduced by replacing Γ_{15} with Γ_7.

III. EXPERIMENTAL EQUIPMENTS AND PROCEDURES

A Q-switched Nd-glass laser (Hadron 104A) was used for the study of GaAs, InP, and ZnTe, and a TEA CO_2 laser was used for InSb. Figure 3 shows the experimental arrangement with the Nd-glass laser. The rotating-prism Q-switched laser was capable of giving light pulses of ~30-nsec halfwidth with a peak power up to 30 MW at 1.06 μm. The laser beam is linearly polarized by a Glen polarizer. The energy of a laser pulse was calibrated by using a ballistic thermopile power meter. The light-pulse shape was monitored by a high-speed silicon photodiode 1 (SGD-100A) and displayed on a fast oscilloscope (Tektronics 454). The light intensity incident on the sample was varied by using attenuators with dielectric coatings. The radiation transmitted by the sample was monitored by photodiode 2, the output of which was fed to the same oscilloscope through a delay cable. The oscilloscope screen showed a trace of two pulses, the incident and the transmitted radiation. The laser beam is not uniform over its cross section. An aperture was used to ensure uniformity of the beam incident on the sample. It was found that by choosing certain areas of the laser beam, the beam passed by the aperture was proportional to the area of the aperture in the range 1–3 mm of aperture radius. An aperture radius 1.5 mm was used. The transmission taken refers to the peak of the two pulses. Measurements were made with power intensities $I \lesssim 25$ MW/cm^2 which was limited by the risk of sample damage. The trace was photographed each time the laser was fired. On the average, five pictures were taken for each power level of the laser. The two-photon absorption coefficient α_2 was deduced from

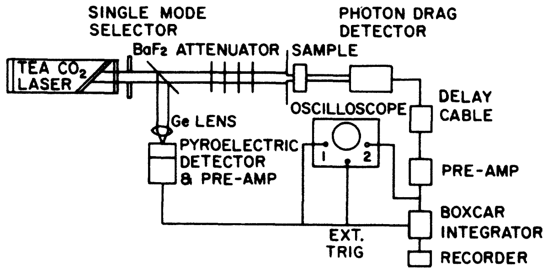

FIG. 4. Experimental setup with the CO_2 laser.

the transmission.

In the measurements using an additional light source, the part of Fig. 3 enclosed in A was replaced by the part shown by dashed lines. The second radiation source was a high-pressure Hg lamp. From the lamp radiation chopped at 13 Hz, monochromatic radiation $\hbar\omega_2$ was obtained using the Leiss spectrometer with a NaCl prism. The $\hbar\omega_2$ radiation transmitted by the sample was detected by a copper-doped-germanium detector at liquid-helium temperature, and fed to a lock-in amplifier (PAR HR-8) and the oscilloscope. Filter 1 (Corning 7-57) in front of the sample cut off the intense visible light from the Hg lamp. Filter 2 (Corning 4-97) blocked the scattered laser radiation. When the laser pulse radiation I_1 fell on the sample, there was a dip of I_2 signal due to the two-photon $(\hbar\omega_1+\hbar\omega_2)$ absorption. Since the dip ΔI_2 was a fast signal, a wide-band amplifier was needed. In order to obtain a reasonable signal-to-noise ratio, the studies were limited to $\lambda \lesssim 3$ μm since I_2 given by the Hg lamp dropped with increasing wavelength.

The experimental setup with the CO_2 laser is shown in Fig. 4. The laser (Gen Tec R-200) was capable of giving 3-MW/cm^2 pulses of unfocused radiation at 10.6 μm with a repetition rate 200 pulses per sec. The half-width of a pulse was ~200 nsec. The beam was linearly polarized by a NaCl Brewster-angle window, and could be adjusted to TEM_{00} mode by means of a single-mode selector. The attenuator consisted of a number of polyester sheets. A few percent of the radiation was reflected by a BaF_2 beam splitter and focused by a Ge lens onto a pyroelectric detector, giving a steady trigger signal. The radiation transmitted by the InSb sample was collected by a photon-drag detector, the output of which was fed to a fast boxcar integrator (PAR 160). A delay cable of ~300 nsec following the detector postponed the arrival of signal from the triggering of the boxcar integrator. In this way, the jitter in triggering due to irregularity in laser firing was eliminated, making the signal given by the boxcar stable and reproducible.

IV. EXPERIMENTAL RESULTS

Consider the case of using only the laser as radiation source, the attenuation of radiation intensity I in the sample is given by

$$-\frac{dI}{dx}\equiv(\alpha+\alpha_2+\alpha_f)I\equiv\alpha I+\beta I^2+aI^3, \tag{53}$$

where α, α_2, and α_f are absorption coefficients due, respectively, to one-photon transitions, two-photon transitions, and transitions of free carriers generated by two-photon absorption. α_2 is proportional to I as can be seen from Eqs. (1) and (3). The free-carrier absorption generated by two-photon absorption is proportional to $\alpha_2 I$. Hence α_f is proportional to I^2. The following expression can be derived easily:

$$\frac{2\beta}{(4a\alpha-\beta^2)^{1/2}}\tan^{-1}\frac{(4a\alpha-\beta^2)^{1/2}[(1-R)I_0-(1-R^2t_0^2)I_t/(1-R)]}{2\alpha+2a(1-R^2t_0^2)I_0I_t+(1-R)\beta I_0+(1-R^2t_0^2)\beta I_t/(1-R)}+2\alpha d$$
$$+\ln\left(\frac{(1-R^2t_0^2)^2I_t^2}{I_0^2}\,\frac{a(1-R)^2I_0^2+\beta(1-R)I_0+\alpha}{a(1-R)^2(1-R^2t_0^2)^2I_t^2+\beta(1-R)^3(1-R^2t_0^2)I_t+(1-R)^4\alpha}\right)=0\,, \tag{54}$$

where $t_0=e^{-\alpha d}$, d is the sample thickness, R is the reflectivity, I_0 is the incident, and I_t is the transmitted intensity. In case α_f is negligible, we get[11]

$$\frac{1}{T}\equiv\frac{I_0}{I_t}=\left(\frac{e^{\alpha d}}{(1-R)^2}+\frac{\beta(e^{\alpha d}-1)}{\alpha(1-R)}I_0\right)\times\frac{1+e^{\alpha d}/R+(e^{\alpha d}/R)^2}{2+e^{\alpha d}/R+(e^{\alpha d}/R)^2}\,, \tag{55}$$

which is a straight line as a function of I_0. The intercept of the straight line gives α and the slope gives β. If α is negligible we get

$$\beta^2 d-\beta\left(\frac{1-R}{(1-R^2t_0^2)I_t}-\frac{1}{(1-R)I_0}\right)-a\ln\left[\left(1+\frac{\beta}{a(1-R)I_0}\right)\Big/\left(1+\frac{\beta(1-R)}{a(1-R^2t_0^2)I_t}\right)\right]=0\,. \tag{56}$$

In the case when Eq. (54) or (56) has to be used, α, α_2, and α_f are to be determined by fitting the curve of reciprocal transmission $1/T$.

Consider the case of two radiations, laser radiation ω_1 and a second radiation of variable frequnecy ω_2. The attenuation of radiation I_2 is given by

$$-\frac{1}{I_2}\frac{dI_2}{dx} \equiv \alpha(\omega_2) + \alpha_{1,2}^{(2)} + \alpha_f(\omega_2) \;, \tag{57}$$

where α is one-photon absorption coefficient at ω_2, $\alpha_{1,2}^{(2)}$ is absorption coefficient due to two-photon $(\hbar\omega_1+\hbar\omega_2)$ absorption, and α_f is the absorption coefficient due to free carriers generated by $2\hbar\omega_1$ and $(\hbar\omega_1+\hbar\omega_2)$ absorption processes. According to Eqs. (1) and (2), we may write

$$\alpha_{1,2}^{(2)} = \beta_{1,2}^{(2)} I_1 \;. \tag{58}$$

α_f is proportional to the concentration of excess electron-hole (e-h) pairs. The e-h pairs generated during a time t is $(\alpha_2 I_1/2\hbar\omega_1 + \alpha_{1,2}^{(2)} I_2/\hbar\omega_2)t$. The e-h recombination may be neglected for a time t shorter than the e-h recombination time. Therefore,

$$\alpha_f \propto (\alpha_2 I_1/2\hbar\omega_1 + \alpha_{1,2}^{(2)} I_2/\hbar\omega_2)t \;. \tag{59}$$

In our experiments $I_2 \ll I_2$ and we have approximately

$$\alpha_f \propto I_1^2 \equiv a I_1^2 \;. \tag{60}$$

The transmission of radiation ω_2 is

$$T = \frac{(1-R)^2 \exp[-(\alpha+\alpha_{1,2}^{(2)}+\alpha_f)d]}{1-R^2\exp[-2(\alpha+\alpha_{1,2}^{(2)}+\alpha_f)d]} \;. \tag{61}$$

In case

$$\frac{1-R^2 e^{-2\alpha d}}{1-R^2\exp[-2(\alpha+\alpha_{1,2}^{(2)}+\alpha_f)d]} \simeq 1 \;, \tag{62}$$

it can be readily shown that

$$(I_1 d)^{-1}\ln(T/T_0) = \beta_{1,2}^{(2)} + a I_1 \;, \tag{63}$$

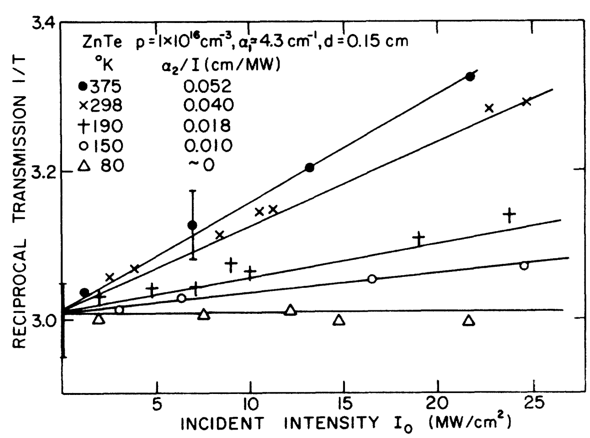

FIG. 5. Reciprocal transmission versus intensity of incident radiation for ZnTe measured at various sample temperatures.

where T_0 is the transmission of radiation of ω_2 in the absence of the laser radiation. In our measurements, Eq. (62) and therefore (63) applies. A short laser pulse was turned on producing a dip $(T_0 - T)$ in the transmission. Using the data, $\beta_{1,2}^{(2)}$ and a were determined according to Eq. (63).

A. ZnTe

Samples of undoped ZnTe single crystals with $p = 1\times10^{16}$ cm^{-3} and $p = 3\times10^{16}$ cm^{-3} were measured in the temperature range 80–375 °K. Figure 5 shows the results obtained for a sample with $p = 1\times10^{16}$ cm^{-3}. The data points for each temperature appear to follow a straight line. The value of α deduced from the intercept on the vertical axis agrees within experimental uncertainty with the value obtained from measurements made with a weak radiation. The uncertainty of the straight line for each temperature is estimated by taking into account the uncertainty of the intercept and the points. The two-photon absorption coefficients α_2 deduced from the straight lines according to (55) are shown by the solid points in Fig. 6. The results obtained for another sample ($p = 3\times10^{16}$ cm^{-3}) are shown by the circles. For ZnTe, $(2\hbar\omega - E_g)$ varies considerably with sample temperature through the temperature dependence of E_g. Figure 6 shows that two-photon absorption was not measurable below 130 °K as is expected since $[2\hbar\omega - (E_g - E_b)] < 0$ for $T \leqslant 130$ °K. The curves I and (1) are calculated theoretically with and without exciton effect, respectively, using Eqs. (3), (33), and (40). The corresponding curves I′ and 1′ are calculated with an additional band Γ_7 using Eqs. (46) and (52). Comparison of I and I′, or 1 and 1′, shows that the effect of the additional band is small. Our data agree well with I or I′. Curves 1 and 1′ calculated without exciton effect are lower by about an order of magnitude, showing the importance of exciton effect. The effect is particularly important where $2\hbar\omega$ is close to E_g as in the case of ZnTe.

B. InSb

A sample of single crystal InSb with $n(77\,°\mathrm{K}) = 3\times10^{14}$ cm^{-3} was measured at room temperature by using a CO_2 laser with polarization parallel to $\langle 111\rangle$. The data are plotted in Fig. 7, giving $\alpha_2/I = 15\pm2$ cm/MW. The experimental and calculated values of α_2/I are listed in Table V which includes the values reported in previous publications and the values obtained in this work. There is considerable discrepancy among previous experimental values for liquid-nitrogen (LN_2) temperature. Our experimental value is in good agreement with the only one previous value reported for room temperature (RT).[6] None of the previous calculations included the exciton effect.

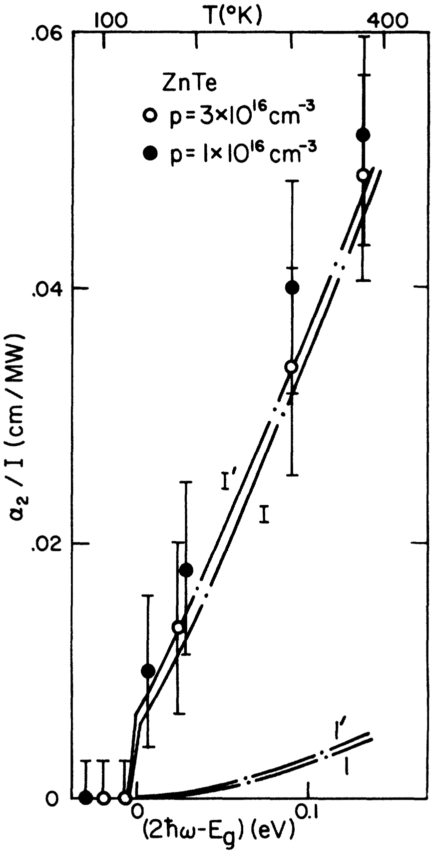

FIG. 6. α_2/I deduced from measurements for the ZnTe sample (open circles for $P=3\times10^{16}$ cm^{-3}, closed circles for $p=1\times10^{16}$ cm^{-3}). Curves I and 1 are calculated theoretically with and without exciton effect. Curves I′ and 1′ are calculated correspondingly with an additional band Γ_7.

One of the calculations[3] was made by assuming a simple valence band, and the calculation involved errors. The other calculation[7] took into account the valence-band degeneracy but neglected the inter-valence-band transitions.

Our calculations show that the exciton effect increases α_2/I by a factor ~2 at RT and ~3 at LN_2 temperature. The value 14.3 calculated with exciton effect for RT agrees well with the experimental results. The two experimental values 0.57 ±0.15 and 0.68 reported previously come close to our value 1.03 calculated with exciton effect at LN_2 temperature. The experimental value 0.12 − 0.24 appears to be too low.

C. GaAs

Four samples of single-crystal n-GaAs with carrier concentrations 1×10^{14}, 2.2×10^{14}, 4×10^{14}, and 4×10^{16} cm^{-3}, respectively, were measured at RT with the Nd-glass laser. The sample with the carrier concentration 2.2×10^{14} cm^{-3} was measured at ~15 °K also. The data are plotted in Fig. 8. The data for each temperature can be fitted by a straight line. The values of α_2/I deduced according to Eq. (55) are plotted against $(2\hbar\omega - E_g)$ in Fig. 9(b). The point deduced from the measurement at ~15 °K corresponds to a different value of $(2\hbar\omega - E_g)$. For comparison, the values reported by other authors from room-temperature measurements are also shown in the figure. Solid curves I and I′ are calculated theoretically with and without the Γ_7 band, respectively. The exciton effect is taken into account; expressions (35)–(37) are used in (33) and Eqs. (50) and (51) are used in (46). Solid curves 1 and 1′ are calculated by neglecting the exciton effect; (35)–(37) are sim-

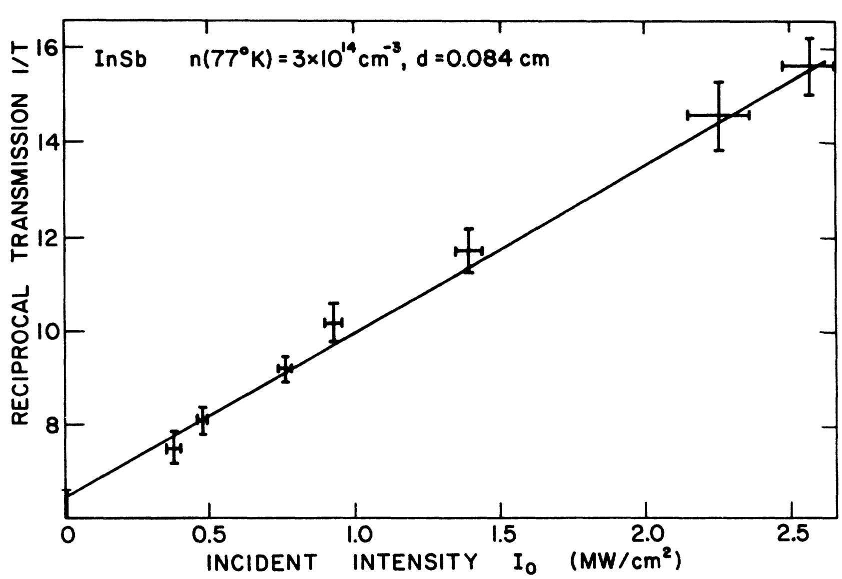

FIG. 7. Reciprocal transmission vs intensity of incident radiation for InSb measured at RT.

TABLE V. Experimental and calculated values of α_2/I (cm/MW) for InSb. The values reported previously and those obtained in this work are listed. The values calculated without exciton effect are given in parentheses.

	Room temperature Expt.	Room temperature Calc.	Liquid N_2 temperature Expt.	Liquid N_2 temperature Calc.
Previous work			0.57 ± 0.15[a]	(1.1[a])
			0.68[b]	
	16 ± 5[c]		~1[c]	
		(6.5)[d]	0.12 – 0.24[e]	(0.24[e])
This work	15 ± 2	14.3		1.03
		(7.6)		(0.31)

[a]Reference 3.
[b]References 4 and 5.
[c]Reference 6.
[d]Calculated according to Ref. 7.
[e]Reference 7.

plified by using (40) and Eqs. (50) and (51) are simplified by using (52). In the calculation of these curves the variation of $(2\hbar\omega - E_g)$ is taken to be due to the variation of E_g at the fixed $\hbar\omega$ of the Nd-glass laser. Our experimental results are several times higher than the calculated curves[27] even the curves including exciton effect. It should be noted that the calculations involve the use of band parameters[28] which may not be applicable for excitation of carriers far away in energy from the band edge.

In order to investigate the exciton effect close to the absorption edge, measurements have been made by combining the Nd-glass laser radiation $\hbar\omega_1$ with a unpolarized radiation of variable frequency $\hbar\omega_2$ to obtain two-photon absorption at $\hbar\omega_1 + \hbar\omega_2$ close to the absorption threshold. The data and calculations on $\alpha_{1,2}^{(2)}$ for RT are shown in Fig. 9(a). The solid curves are for GaAs. Curves I and II are calculated with exciton effect, I for $\hat{\epsilon}_1 \parallel \hat{\epsilon}_2$, and II for unpolarized ω_2. Curves 1 and 2 are calculated correspondingly without exciton effect. Our data were measured with unpolarized ω_2. The data are in fair agreement with curve II, showing that the calculation indeed applies provided the two-photon energy is not too much higher than E_g. Curve 2 is lower than curve II by a factor ~2 and it appears to be too low in comparison with the data. The recently reported value[14] of α_2/I being 0.033 ± 0.015 cm/MW measured on several samples with a Nd-YAG laser with $\hbar\omega = 0.94$ eV supports this conclusion. Calculation with exciton effect gives $\alpha_2/I = 0.05$ cm/MW for $(2\hbar\omega - Eg) = (1.88 - 1.435)$ eV $= 0.455$ eV, which is close to the measured value.

D. InP

Measurements were made on single crystal[29] and polycrystalline samples of InP. The data are shown in Fig. 10. The reciprocal transmission increased faster than linearly with radiation intensity. We have checked[11] by photoconductivity measurements that this behavior is the consequence of significant absorption by free carriers produced by the two-phonon transitions. The values of α, β, and a deduced according to Eqs. (54) and (56) are listed in Table VI. The values of α given by the intercepts of the curves in Fig. 10 agree with one-photon absorption coefficients measured with weak intensity of radiation. The values of a are

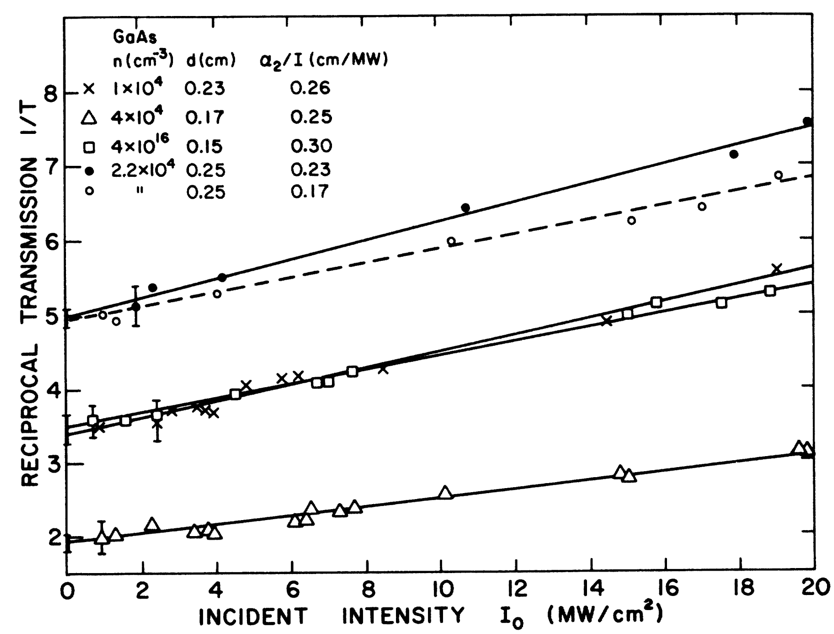

FIG. 8. Reciprocal transmission vs intensity of incident radiation for various GaAs samples. Solid lines are for RT. Dashed line is for ~15 °K.

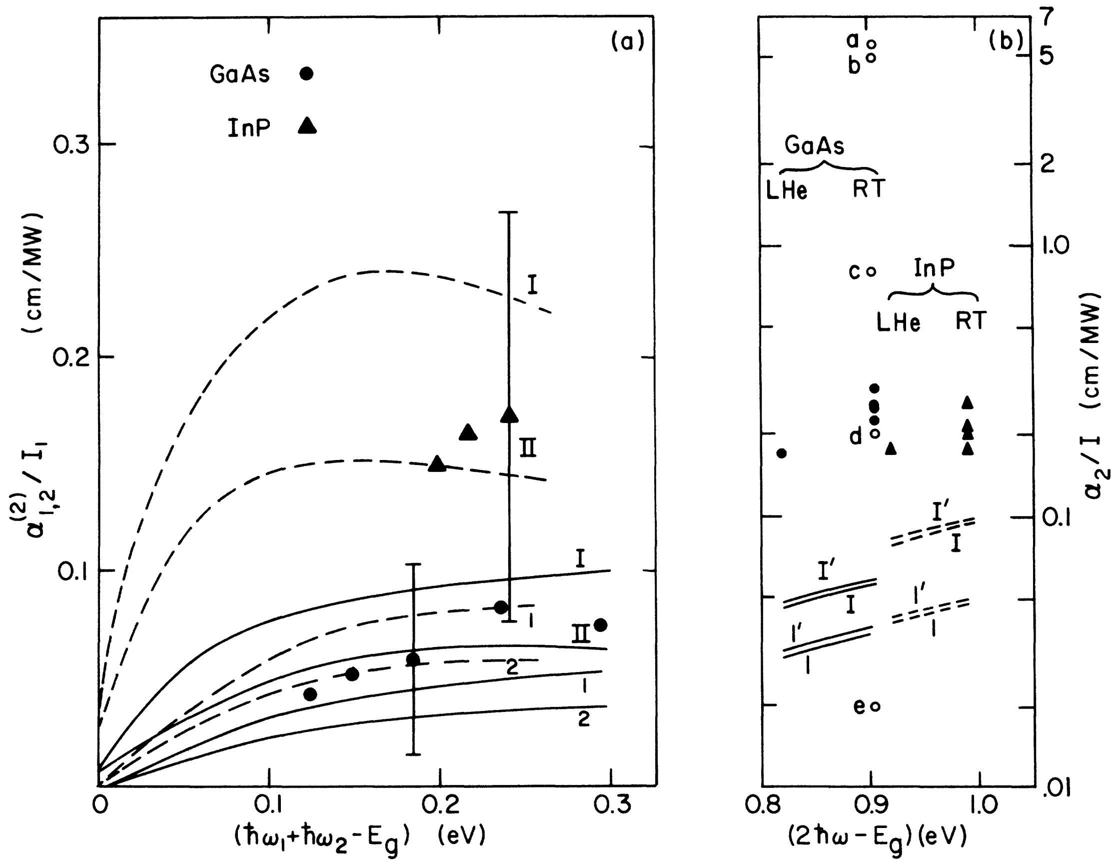

FIG. 9. (a) $\alpha^{(2)}_{1,2}/I_1$ vs $(\hbar\omega_1+\hbar\omega_2-E_g)$, measured at RT. Closed circles for GaAs ($n=4\times10^{16}$ cm^{-3}) and closed triangles for InP ($n=2\times10^{16}$ cm^{-3}). Solid and dashed curves are calculated for GaAs and InP, respectively. I and II are calculated with exciton effect for polarized ($\hat{e}_2 \parallel \hat{e}_1$) and unpolarized ω_2 radiation, respectively. 1 and 2 are corresponding curves calculated without exciton effect. (b) α_2/I vs $(2\hbar\omega-E_g)$ measured for GaAs and InP at RT and LHe temperature. Curves I and 1 are calculated theoretically with and without exciton effect, respectively. Curves I′ and 1′ are calculated including the additional band Γ_7. The open-circle data points are experimental results for GaAs from previous publications: a, Ref. 12; b, Ref. 8; c, Ref. 9; d, Ref. 13; e, Ref. 10.

consistent with free-carrier absorption and two-photon-produced concentration given by photoconductivity studies. The data of α_2/I plotted in Fig. 9(b) are seen to lie above the dashed curves I and I′ calculated with exciton effect included by a factor of ~2. Following considerations similar to that in the case of GaAs, measurements were made with an additional radiation ω_2. Figure 9(a) shows that the data of $\alpha^{(2)}_{1,2}/I_1$ agree reasonably with the dashed curve II which takes into account the exciton effect. Again, the dashed curve 2 calculated with omission of exciton effect seems to be too low.

TABLE VI. Experimental values of α, β, a for InP.

	n (cm^{-3})	d (cm)	α (cm^{-1})	$\beta\equiv\alpha_2/I$ (cm/MW)	$a\equiv\alpha_f/I^2$ (cm^3/MW^2)
1	2×10^{16}	0.182	0.6	0.26 ± 0.13	0.15 ∓ 0.05
2	1×10^{16}	0.186	0.2	0.20 ± 0.10	0.15 ∓ 0.05
3	1×10^{17}	0.577	0.6	0.21 ± 0.09	0.15 ∓ 0.06
4	1×10^{17}	0.577	~0	0.18 ± 0.09	0.13 ∓ 0.06

TABLE VII. Calculated and experimentally determined values of two-photon absorption α_2/I and $\alpha^{(2)}_{1,2}/I_1$ (cm/MW) for RT are listed for the four materials studied.

	ZnTe	InSb	GaAs		InP	
$2\hbar\omega-E_g$(eV)	0.090	0.054	0.905		0.99	
$\hbar\omega_1+\hbar\omega_2-E_g$(eV)				0.145		0.23
(cm/MW)	α_2/I	α_2/I	α_2/I	$\alpha^{(2)}_{1,2}/I_1$	α_2/I	$\alpha^{(2)}_{1,2}/I_1$
Simple VB						
no exciton	0.0004	1.6	0.005	0.007	0.006	0.015
exciton	0.0018	2.3	0.007	0.014	0.009	0.028
Degenerate VB						
no exciton	0.0025	7.6	0.039	0.031	0.050	0.058
exciton	0.0317	14.3	0.058	0.062	0.096	0.147
Experiment	0.034	15	0.23	0.05	0.21	0.17

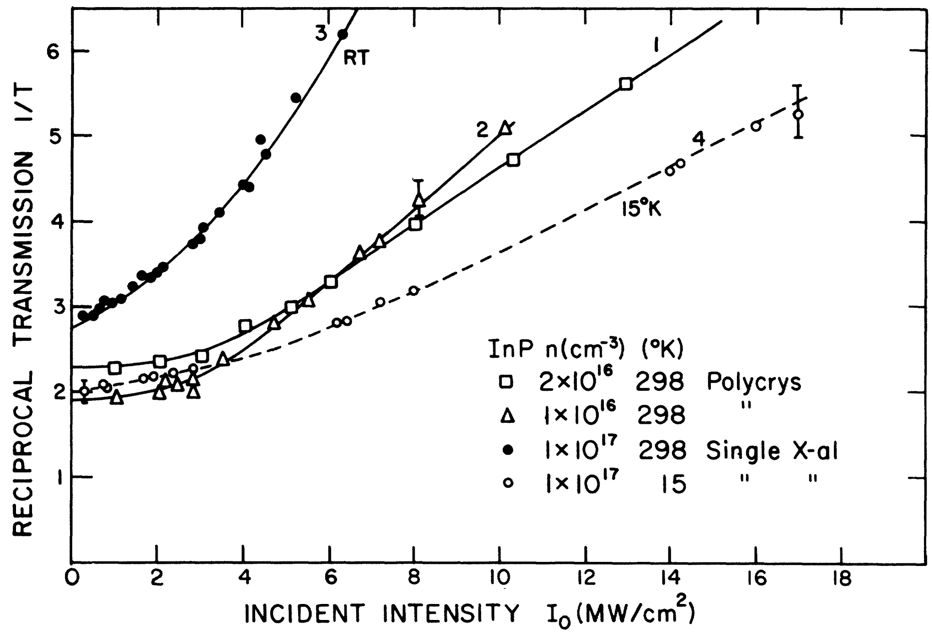

FIG. 10. Reciprocal transmission vs intensity of incident radiation for various InP samples. Solid lines are for RT. Dashed line is for ~15 °K.

V. SUMMARY

Some of the experimental and calculated values of α_2/I and $\alpha_{1,2}^{(2)}/I_1$ are summarized in Table VII. The importance of degeneracy of the valence band is indicated by the comparison of values calculated with and without the degeneracy. The valence-band degeneracy increases the calculated α_2/I and $\alpha_{1,2}^{(2)}/I_1$ by a factor given approximately by Eq. (42). The effect of individual branches of the degenerate valence band add together. Moreover, inter-valence-band transitions are added.

The importance of taking into account exciton effect can be seen by comparing the values calculated with and without the exciton effect. The exciton effect increases two-photon abosrption by the factor (41). The fact that this factor is larger for larger X_1 can be easily seen by comparing the effects of ZnTe and InSb. For ZnTe with $X_1=0.48$, α_2/I is increased by a factor of ~12.6, whereas for InSb with $X_1=0.09$, α_2/I is increased by only a factor of ~1.9. For all materials, the value calculated with the exciton effect for degenerate valence band is close to the experimental values, provided the two-photon energy is not too high compared to E_g. The discrepancy between the calculated and experimental values of α_2/I for GaAs and InP at a large $(2\hbar\omega - E_g)$ may be an indication that the calculation ceases to be a good approximation when energy states deep in the bands are involved. The existence of energy bands far removed in energy from the conduction and valence bands does not affect two-photon absorption strongly. The effect of the band Γ_7 which is closest in energy in these materials is given by Eq. (46). The effect is small as can be seen in Figs. 6 and 9.

*Work supported in part by the Office of Naval Research.

[1]For CdS, see R. Braunstein and N. Ockman, Phys. Rev. 134, A499 (1964); R. J. Regensburger, E. Panizza, Phys. Rev. Lett. 18, 113 (1967); M. S. Bespalov, L. A. Kulevskii, V. P. Makarov, M. A. Prokhorov, and A. A. Tikhonov, Zh. Eksp. Teor. Fiz. 55, 144 (1968) [Sov. Phys.-JETP 28, 77 (1969)]; F. Pradere and A. Mysyrowicz, in Proceedings of the Tenth International Conference on the Physics of Semiconductors, Cambridge, 1970, p. 101. For CdSe, see A. Z. Grasyuk, I. G. Zubarev, and A. N. Mentser, Fiz. Tverd. Tela 10, 543 (1968) [Sov. Phys.-Solid State 10, 427 (1968)]. For CdTe, see J. M. Ralston and R. K. Chang, Appl. Phys. Lett. 15, 164 (1969). For ZnS, see E. Panizza, Appl. Phys. Lett. 10, 265 (1967). For GaP, see B. M. Ashkinadze *et al.* in *Proceedings of the Ninth International Conference on the Physics of Semiconductors*, edited by S. M. Ryvkin (Nauka, Leningrad, 1968), p. 189. For Si, see J. Sevin and G. Mayer, C. R. Acad. Sci. Paris B 264, 1369 (1967); J. M. Ralston and R. K. Chang, Opto Elect. 1, 182 (1969); J. F. Reintjes and J. C. McGrody, Phys. Rev. Lett. 30, 901 (1973).

[2]A. F. Gibson, M. J. Kent, and M. F. Kimmitt, Brit. J. Appl. Phys. 1, 149 (1968).

[3]A. M. Danishevskii, A. A. Patrin, S. M. Ryvkin, and L. D. Yaroshetskii, Zh. Eksp. Teor. Fiz. 56, 1457 (1969) [Sov. Phys.-JETP 29, 781 (1969)].

[4]C. K. N. Patel, P. Fleury, R. Slusher, and H. Frisch, Phys. Rev. Lett. 16, 971 (1966).

[5]R. E. Slusher, W. Giriat, and S. R. J. Brueck, Phys. Rev. 183, 758 (1969).

[6]J. M. Doviak, A. F. Gibson, M. F. Kimmitt, and A. C. Walker, J. Phys. C 6, 593 (1973).

[7]H. J. Fossum and D. B. Chang, Phys. Rev. B 8, 2842 (1973).

[8]N. G. Basov, A. Z. Gresyuk, I. G. Zubarev, V. A. Katulin, and O. N. Krokhin, Zh. Eksp. Teor. Fiz. 50, 551 (1966) [Sov. Phys.-JETP 23, 366 (1966)]; N. G. Basov, A. Z. Grasyuk, V. F. Efimkov, I. G. Zubarev, V. A. Katulin, and Ju. M. Popov, J. Phys. Soc. Jap. Suppl. 21, 277 (1966).

[9]V. V. Arsen'ev, V. S. Dneprovskii, D. N. Klyshko, and A. N. Penin, Zh. Eksp. Teor. Fiz. 56, 760 (1969) [Sov. Phys.-JETP 29, 413 (1969)].

[10]J. M. Ralston and R. K. Chang, Appl. Phys. Lett. 15, 164 (1969).

[11]C. C. Lee and H. Y. Fan, Appl. Phys. Lett. 20, 18 (1972).

[12]Jayaraman and C. H. Lee, Appl. Phys. Lett. 20, 392 (1972).

[13]Ya. A. Oksman, A. A. Semenov, V. N. Smirnov, and O. M. Smirnov, Fiz. Tekh. Poluprovodn. 6, 731 (1972) [Sov. Phys.-Semicond. 6, 629 (1972)].

[14]D. A. Kleinman, R. C. Miller, and W. A. Nordland, Appl. Phys. Lett. 23, 243 (1973).

[15]L. V. Keldysh, Zh. Eksp. Teor. Fiz. 47, 1945 (1964) [Sov. Phys.-JETP 20, 1307 (1965)].

[16]R. Braunstein, Phys. Rev. 125, 475 (1962); R. Braunstein and N. Ockman, Phys. Rev. 134, A499 (1964).

[17]R. Loudon, Proc. R. Soc. Lond. 80, 952 (1962).

[18]G. D. Mahan, Phys. Rev. Lett. 20, 332 (1968); G. D. Mahan, Phys. Rev. 170, 825 (1968).

[19]A. Baldereschi and N. O. Lipari, Phys. Rev. Lett. 25, 373 (1970); Phys. Rev. 3, 439 (1971).

[20]F. H. Pollak, C. W. Higginbotham, and M. Cardona, J. Phys. Soc. Jap. Suppl. 21, 20 (1966); B. Segall, in *Physics and Chemistry of II-VI Compounds*, edited by M. Aven and J. Prener (North-Holland, Amsterdam, 1967), p. 1.

[21]E. O. Kane, J. Phys. Chem. Solids 1, 249 (1957).

[22]G. Dresselhaus, J. Phys. Chem. Solids 1, 14 (1956); J. O. Dimmock, in *Semiconductors and Semimetals*, edited by R. K. Willardson and A. C. Beer (Academic, New York, 1967), Vol. 3, p. 259.

[23]G. Dresselhaus, A. F. Kip, and C. Kittel, Phys. Rev. 98, 368 (1955).

[24]N. O. Lipari and A. Baldereschi, Phys. Rev. B 6, 3764 (1972).

[25]R. J. Elliott, in *Polarons and Excitons*, edited by C. G. Kuper and G. D. Whitfield (Oliver and Boyd, London, 1963), p. 269.

[26]M. I. Bell, in *Electronic Density of States*, edited by L. H. Bennett, U. S. Natl. Bur. Std. Spec. Publ. No. 323 (U. S. GPO, Washington, D.C., 1971), p. 757.

[27]In a preliminary report, Ref. 11, a value of $\alpha_2/I = 0.02$ cm/MW calculated without exciton effect was given. That value was calculated according to an expression given by Basov *et al.* (Ref. 8) with some numerical corrections. Curve 1 in Fig. 9(b) was calculated by using Kane's wave functions and including inter-valence-band transitions. The value of α_2/I at RT is 0.039 cm/MW.

[28]M. Cardona, J. Phys. Chem. Solids 24, 1543 (1963).

[29]The single-crystal ingot InP was kindly supplied by Dr. J. Woodall of IBM Watson Research Center.